025921-32-T

Semiannual Progress Report

P-44

National Aeronautics and Space Administration
Ames Research Center
Moffett Field CA 94035

Pacific Missile Test Center
Pt. Mugu CA 93042-5000

September 1992

THE UNIVERSITY OF MICHIGAN
Radiation Laboratory
Department of Electrical Engineering
and Computer Science
Ann Arbor, Michigan 48109-2122
USA

025921-32-T

TECHNICAL REPORT

for NASA Grant NAG-2-541

NASA Technical Monitor: Alex Woo

Grant Title:	Development of 3D Electromagnetic Modeling Tools for Airborne Vehicles
Report Title:	Semiannual Progress Report
Institution:	Radiation Laboratory Department of Electrical Engineering and Computer Science The University of Michigan Ann Arbor MI 48109-2122
Period Covered:	February 1992 – September 1992
Principal Investigator:	John L. Volakis Volakis@um.cc.umich.edu Telephone: (313) 764-0500

Table of Contents

Objective

Currently no software simulations are available from industry or academia which can allow an accurate computation of the radar signature from full scale non-metallic vehicles primarily because existing formulations have excessive memory and computational demands in addition to being unsuitable for modern machine architectures. Such software are required for test and evaluation purposes of future aircraft systems/platforms, target simulation platforms, on-board communication systems and for radar signature evaluation.

Traditional methodologies for radar signature or performance analysis of on-board communication systems have not shown any promise in simulating large scale composite vehicles. Furthermore, approximate simulation techniques are of no utility in modeling complex, composite structures. The intent of this research is thus aimed at developing new methodologies which will allow accurate and efficient simulations of full scale vehicles. We propose to accomplish this with the development of algorithms which have very low memory requirements and make use of recent advances in high performance and parallel computing. The particular technique to be employed is a hybrid version of the finite element method which has been successfully implemented and tested at the University of Michigan for two-dimensional applications. Also, some three dimensional results relating to specific scattering and antenna configurations have verified our expectations of the method's potential. The basis of this approach is to reformulate an open-boundary problem into a closed-boundary one using a mesh termination method which brings the outer boundary very close to the body. Segmentation and connectivity schemes can then be employed to subdivide the system/volume into smaller (of any number) sections which can be independently treated by separate single or parallel processors. Except for the small Toeplitz connectivity matrices, all others are sparse and banded, making their solution convenient, and since there is no need for concurrent storage of any of these submatrices, there is no limitation on the size of the computational domain, a problem which has become the bottleneck in computational electromagnetics. It is thus our claim that this solution approach, coupled with the advantages of the finite element method, will make a dramatic impact in the field of numerical electromagnetics, and promises to provide the necessary future tools for numerous applications, including target simulation, radar signature analysis and imaging, antenna modeling and VLSI circuit simulations.

Progress

As stated above, the main goal of this project is to develop methodologies for scattering by airborne composite vehicles. Although our primary focus continues to be the development of a general purpose code for analyzing the entire structure as a single unit, a number of other tasks are also pursued in parallel with this effort. These tasks, are important in testing the overall approach and in developing suitable models for materials coatings, junctions and, more generally, in assessing the effectiveness of the various parts comprising the final code.

Below we briefly discuss our progress on the five different tasks which were pursued during this period. Our progress on each of these tasks is described in the detailed reports (listed at the end of this report) and the memoranda included with this document. The first task described below is, of course, the core of this project and deals with the development of the overall code. Undoubtedly, it is the outcome of the research which was funded by NASA-Ames and the Navy over the past three years.

Task: Three-dimensional hybrid finite element formulation for scattering

During this year we developed the first finite element code for scattering by structures of arbitrary shape and composition. The code employs a new absorbing boundary condition which allows termination of the finite element mesh only 0.3λ from the outer surface of the target. This leads to a remarkable reduction of the mesh size and is a unique feature of the code. Other unique features of this code include capabilities to model resistive sheets, impedance sheets and anisotropic materials. This last capability is the latest feature of the code and is still under development.

The code has been extensively validated for a number of composite geometries and some examples are given in Figures 1 and 2. The validation of the code is still in progress for anisotropic and larger non-metallic geometries and cavities.

The developed finite element code is based on a Galerkin's formulation and employs edge-based tetrahedral elements for discretizing the dielectric sections and the region between the target and the outer mesh termination boundary (ATB). This boundary is placed in conformity with the target's outer surface thus resulting in additional reduction of the unknown count.

The resulting system is symmetric and is solved via an iterative biconjugate gradient algorithm. It is particularly important to note that only the non-zero elements of the sparse matrix system. In this manner, the achieved storage requirement is $30N$. The edge based elements lead to matrices which have greater bandwidths but are sparser and the employed storage scheme takes advantage of this sparsity. In contrast to the node-based elements which have been traditionally used in aerodynamics, the edge-based elements are better suited for electromagnetic computations. These Witney form-1 elements maintain tangential field continuity and avoid specification of the field at metallic corners. This is crucial because certain field components become undefined at metallic corners.

Over the last few months we have concentrated on the parallelization of the developed finite element code FEMATS. More specifically, the code was ported on our recently acquired Kendall Square multiprocessor facility equipped with 32 processors. At the moment, we have achieved a 23-fold speed-up demonstrating that the code is fully parallelizable using syntactic means. In the future, we shall couple syntactic parallelization with other means of parallelization based on the physical characteristics of the problem and associated formulation.

In addition to the aforementioned unique analytical features of the code, we have also concentrated on user-oriented interface features. Specifically, the code is currently interfaced with the commercial mesh generation package IDEAS marketed by SDRC. This package has graphical interface for building and meshing geometries of arbitrary shape with look-up tables for material specifications. The Universal geometry file generated by IDEAS is read by a preprocessor which recasts the geometry data in a form suitable for the solver. Various postprocessors can be interfaced with the solver for displaying the near-zone fields and far-zone patterns in color coded form for diagnostic purposes. Postprocessors included in the IDEAS package, apE or grafic have been used for data display. To demonstrate this capability a 2-minute video animation was generated displaying the near and far zone fields of an aircraft wing as a function of incidence angle. This video was distributed to NASA-Ames and Pacific Missile Test Center technical monitors of this project.

Task: Hybrid finite element method for a body of revolution

The body of revolution code was completed this year with the delivery of a detailed technical report 025921-31-T describing the formulation and results based on the developed code. Several scattering patterns for coated

and uncoated bodies of revolutions are included in this report which validate the code and demonstrate its capabilities. A unique feature of this code is the combined finite element and boundary integral formulations employed in the implementation. The finite element formulations permit modeling of inhomogeneous materials, whereas the boundary integral acts as an exact mesh termination scheme. The mesh can therefore be terminated very close to the target thus minimizing the unknown count. The drawback of the boundary integral scheme is that it leads to a full submatrix which must be handled carefully for memory reductions. As done in our previous implementations of the finite element method, the boundary integral is cast in convolutional form and this leads to an $O(n)$ memory demand of the overall FE-BI system. Much effort was devoted to the careful computation and implementation of the boundary elements and details pertaining to this are described in the aforementioned report. More recently we concentrated on the application of the code to scattering by coated BOR structures and some examples are shown in figures 3 and 4. In particular, figure 3 displays the effectiveness of a recently developed scheme for suppressing the exterior/interior resonances associated with any solution employing a closed boundary integral formulation. Figure 4 displays the scattering pattern by a coated cone frustrum. As seen the results of our FE-BI code are in good agreement with the moment method. A particular characteristic and advantage of the FE-BI method is its capability to easily treat surface details and inhomogeneous materials.

Task: New impedance wedge diffraction coefficients

Sometime ago we reported in the University of Michigan report 025921-4-T a new approximate impedance wedge diffraction coefficient for characterizing the diffraction by an impedance wedge. We resorted to an approximate coefficient only because the impedance wedge is not amenable to an exact solution when excited by a wave incident in a plane other than that normal to the wedge. This diffraction coefficient was later implemented and successfully tested in a traditional PTD code under a contract supported by the U.S. Army (see University of Michigan report 028371-1-F).

After several applications, the aforementioned diffraction coefficient was found to be at times inaccurate for computing the cross polarization fields. To remedy this deficiency, we examined the possibility of a more rigorous development for the proposed diffraction coefficients. From the start, this effort proved challenging but we have now arrived at a procedure which has yielded a more accurate diffraction coefficient. The new diffraction

coefficient is composed of three different ones, each valid at certain regions of interest as illustrated in figure 5. The validity regime of each of these is based on the specific approximations made in the derivation process and details pertaining to this as given in the technical report 025921-30-T. A chapter is also included in this report providing an extensive validation of the diffraction coefficients for different wedge angles and face impedances. These comparisons clearly show the derived diffraction tensors are very accurate. Examples of the comparisons are shown in figures 6 and 7. On these figures, the new solution is termed as "1st Order Approx. GTD". The indicated differences observed in the shown comparisons are attributed to multiple interactions, and do not therefore burden the developed diffraction coefficients. It is worth pointing out that the derived diffraction coefficients reduce to the known tensors for the wedges having included angles of 0 and 180 degrees.

Task: New finite element formulations for electromagnetic modeling

In our last semi-annual report we reported of a finite element formulation using new solution-aware expansion functions. At that time, we had completed a two-dimensional implementation of this formulation. The three-dimensional implementation is now nearly complete and we shall intially consider its application to inlet and guided structures. For inlets having canonical cross-sections, the finite element method will be implemented with the guided modes serving as the basis functions in constructing the sparse system of equations. This should allow the simulation of long inlets since fine meshing will only be required at the inlet mouth, the engine face and at irregular bends of the inlet geometry not conforming to some canonical shape. This implementation will serve as a demonstration of the method's capability to model large inlet structures. The next step will be the implementation of the method to inlet structures whose shape may be considered as a perturbation of some canonical geometry. In the case of inlets having arbitrary cross section we will consider an implementation based on a combined finite element-high frequency implementation. That is, the fields in the guided region of the inlet structure will be formulated using a ray representation, whereas the regions near the inlet lip and the engine face will be, as before, fine meshed in the usual manner.

Task: New integral equations for scattering by coated structures

Thin material coatings are nowadays routinely used in the construction of all airborne vehicles. Nevertheless, their electromagnetic characterization in the context of integral equations still relies on the use of the simple but less accurate impedance boundary conditions. On the other hand, although finite element formulations can readily deal with the presence of material coatings, their implementation is inefficient when the coating becomes thin. This is because very small elements must be used in the vicinity of the thin coating.

To avoid the inaccuracy of the impedance boundary condition and the inefficiency of the finite element method for modeling thin coatings, a new integral equation was derived and discretized for implementation. The derivation of the new integral equation is described in the University of Michigan technical report 025921-25-T entitled "Alternative field representations and integral equations for modeling inhomogeneous dielectrics". In comparison with traditional integral equations which require as many as eight unknowns in their discretization, the new integral equations requires only three unknowns per cell without any compromise in accuracy. The approximate integral equation based on the impedance boundary condition requires four unknowns per cell. In addition the new integral equation is also associated with a lower kernel singularity which greatly facilitates its discretization. A code based on this formulation has been written and validated. A short report pertaining to the formulation and results obtained from this code are described in the included memorandum.

List of Reports Distributed This Year (1991-92)

1. A. Chatterjee, J.M. Jin and J.L. Volakis, "Application of Edge Based Finite Elements and Vector ABCs in 3D Scattering," University of Michigan Radiation Laboratory Technical Report No. 025921-24-T, Jan. 1992.

2. J.L. Volakis, "Alternative Field Representations and Integral Equations for Modeling Inhomogeneous Dielectrics," University of Michigan Radiation Laboratory Technical Report No. 025921-25-T, Feb. 1992.

3. J.D. Collins and J.L. Volakis, "Progress on Hybrid Finite Element Methods for Scattering by Bodies of Revolution, " Univ. of Michigan Radiation Laboratory Technical Report No. 025921-26-T, Feb. 1992.

4. J.M. Jin, J.L. Volakis, C.L. Yu and A.C. Woo, "Modeling of Resistive Sheets in Finite Element Solutions," Univ. of Michigan Radiation Laboratory Technical Report No. 025921-27-T, Feb. 1992.

5. J.L. Volakis, "Semi-annual Progress Report for NASA Grant NAG-2-541," University of Michigan Radiation Laboratory Technical Report No. 025921-28-T, Jan. 1992.

6. A. Chatterjee, J.M. Jin and J.L. Volakis, "Edge-Based Finite Elements and Vector ABCs applied to 3D Scattering," Radiation Laboratory Report 025921-29-T, May 1992, 18 pp.

7. H.H. Syed and J.L. Volakis, "Electromagnetic Scattering by Coated Convex Surfaces and Wedges Simulated by Approximate Boundary Conditions," Univ. of Michigan Radiation Laboratory Report 025921-30-T, June 1992, 159 pp.

8. J.D. Collins and J.L. Volakis, "A Finite Element-Boundary Integral Method for Electromagnetic Scattering," Univ. of Michigan Radiation Laboratory Report 025921-31-T, June 1992, 157 pp.

Conference Papers as a Result of This Research (1991-92)

1. J.L. Volakis and J.M. Jin, "Radiation and Scattering Analysis of Microstrip arrays via a Hybrid finite element method," 1991 Int. Conference on Electromagnetics in Aerospace Applications (ICEAA), Torino, Italy, Digest pp. 195-198.

2. J.L. Volakis, A. Alexanian, J.M. Jin and C.L. Yu, "Radar Cross Section Analysis and Control of Microstrip Patch Antennas," 1992 IEEE AP-S International Symposium, Chicago, IL, pp. 1645-1648.

3. J.M. Jin, J.L. Volakis and C.L. Yu, "Scattering and Radiation Analysis of Three-Dimensional Cavity Arrays via a Hybrid Finite Element Method," 1992 Radio Science Meeting, Chicago, IL, Digest pp. 573.

4. J.D. Collins and J.L. Volakis, "Characterization of a Class of Axially Symmetric Radomes Using the Finite Element-Boundary Integral Technique," 1992 Radio Science Meeting, Chicago, IL, Digest p. 235.

5. J.L. Volakis and S. Bindiganavale, "A New Three-Dimensional Integral Equation for Modeling Thin Ferrite Coatings On Conductors," 1992 Radio Science Meeting, Chicago, IL, Digest p. 426.

6. A. Chatterjee, J.M. Jin and J.L. Volakis, "Application of Edge-Based Finite Elements and Vector ABCs in 3D Scattering," 1992 IEEE AP-S International Symposium, Chicago, IL, Digest pp. 528-531.

7. H.H. Syed and J.L. Volakis, "Equivalent Current Formulation for an Impedance Wedge of Arbitrary Included Angle," 1992 IEEE AP-S International Symposium, Chicago, IL, Digest pp. 1857-1860.

8. J. Collins, J.M. Jin and J.L. Volakis, "Eliminating Interior Resonances in a Finite Element-Boundary Integral Solution of Scattering Problems," 1992 Conf. on Electromagnetic Field Computation, Claremont, CA.

Papers in Refereed Journals as a Result of This Research (1991-92)

1. H.H. Syed and J.L. Volakis, "An Approximate Diffraction Coefficient for an Impedance Wedge at Skew Incidence," *Electromagnetics*, Vol. 12, No.1, pp. 33-55, 1992.

2. J.L. Volakis, "Alternative Field Representations and Integral Equations for Modeling Inhomogeneous Dielectrics,"*IEEE Trans. Microwave Theory Tech.*, pp. 604-608, March 1992.

3. K. Barkeshli and J.L. Volakis, "Scattering by Filled Grooves and Slits," *J. of Electromagnetic Waves and Applications*, Vol. 6, No.4, pp. 459-474, 1992.

4. J.M. Jin and J.L. Volakis, "A Biconjugate Gradient FFT Solution for Scattering by Planar Plates," *Electromagnetics,* Vol. 12, No.1, pp. 105-119, 1992.

5. M.A. Ricoy and J.L. Volakis, "Diffraction by a Symmetric Material Junction Using Higher Order Impedance Boundary Conditions," *IEEE Trans. Antennas and Propagat.*, July 1992.

6. J.M. Jin, J.L. Volakis, C.L. Yu and A. Woo, "Modeling of Resistive Sheets in the Context of Finite Element Solutions," *IEEE Trans. Antennas and Propagat.*, Vol. 40, pp. 727-731, June 1992.

7. A. Chatterjee, J.M. Jin and J.L. Volakis, "Computation of Cavity Resonances Using Edge-Based Finite Elements," *IEEE Trans. Microwave Theory Techn.*, Nov. 1992.

8. J.M. Jin and J.L. Volakis, "A Fictitious Absorber For Truncating Finite Element Meshes in Scattering," accepted in *IEE Proceedings, Part H.*, 1992.

9. J.-M. Jin and J.L. Volakis, "A Unified Approach to Integral Equation Formulations for Electromagnetic Scattering," submitted to *J. of Electromagnetic Waves and Applications.*

10. L. Kempel, J.L. Volakis and T.B.A. Senior, "TM Scattering from Tapered Resistive Junctions," accepted in *Radio Science.*

11. J.L. Volakis and J.M. Jin, "A Technique to Substantially Lower the Resonant Frequency of the Microstrip Patch Antenna," *IEEE Trans. Microwave Theory and Techn. Letters,* Vol. 2, No. 7, pp. 292-293, July 1992.

12. J.D. Collins, J.M. Jin and J.L. Volakis, "Eliminating Interior Cavity Resonances in Finite Element-Boundary Integral Methods for Scattering," accepted in *IEEE Trans. Antennas Propagat.*

13. A. Chatterjee, J.M. Jin and J.L. Volakis, "A Robust Finite Element Formulation for Three Dimensional Scattering," *IEEE Electronics Letters*, Vol. 28, No. 10, pp. 966-967, 1992.

14. A. Chatterjee, J.M. Jin and J.L. Volakis, "A Finite Element Formulation with Absorbing Boundary Conditions for Three Dimensional Scattering," submitted to *IEEE Trans. Antennas Propagat.*

15. H.H. Syed and J.L. Volakis, "On the Skew Incidence Diffraction of an Impedance Wedge with Arbitrary Face Impedances," submitted to *Radio Science.*

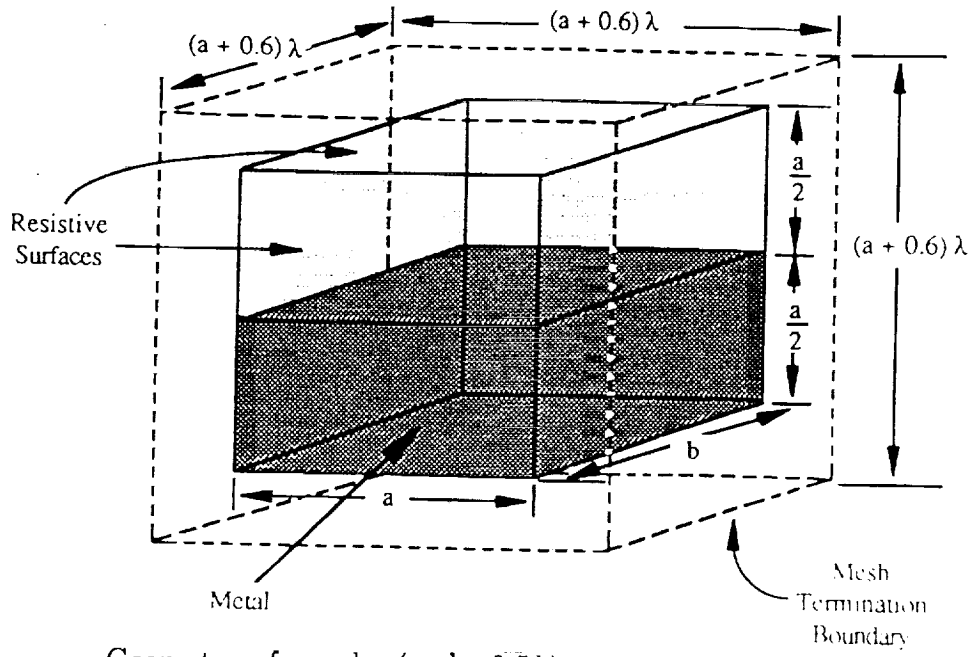

Geometry of a cube (a=b=0.5λ) consisting of a metallic section and an air-filled section, where the latter is bounded by a resistive surface having $R = Z_o$. The outer cube drawn with dashed lines represents the surface on which the ABC was enforced.

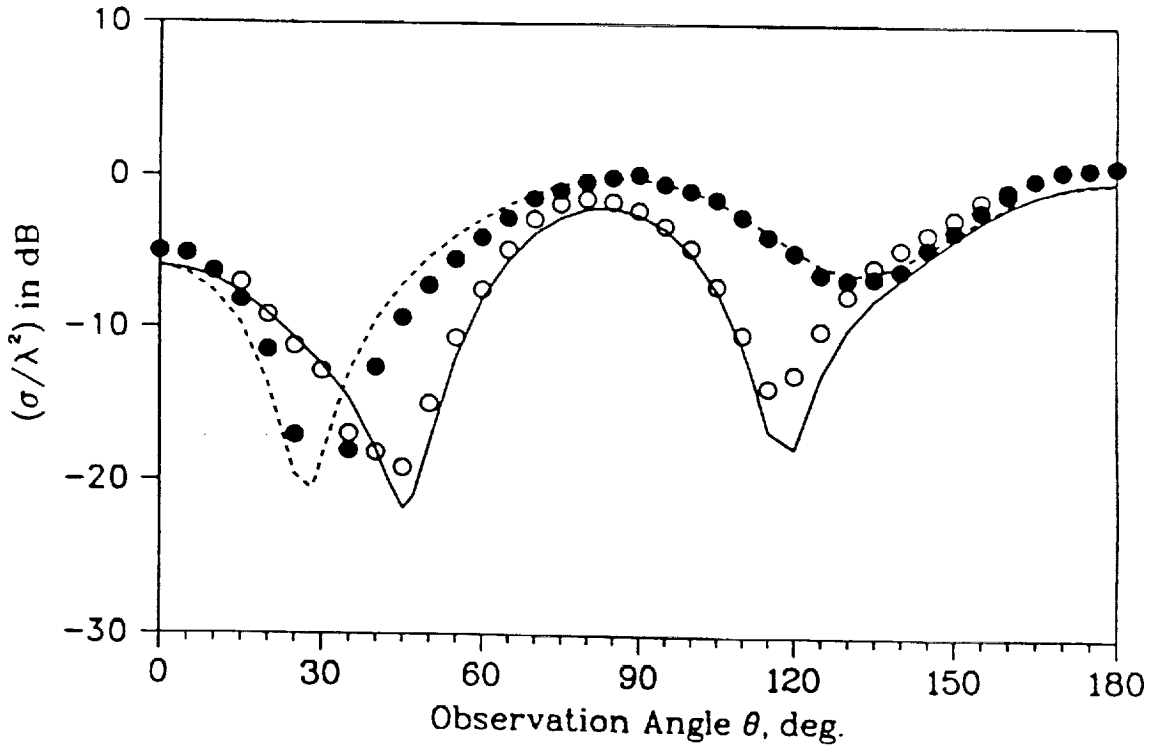

Figure 1: RCS patterns in the x-z plane for the shown geometry with $H_z^{\text{inc}} = 0$ (solid curve is the FE-ABC pattern; circles are MOM data) and $E_z^{\text{inc}} = 0$ (dashed curve is the FE-ABC pattern; black dots are MOM data).

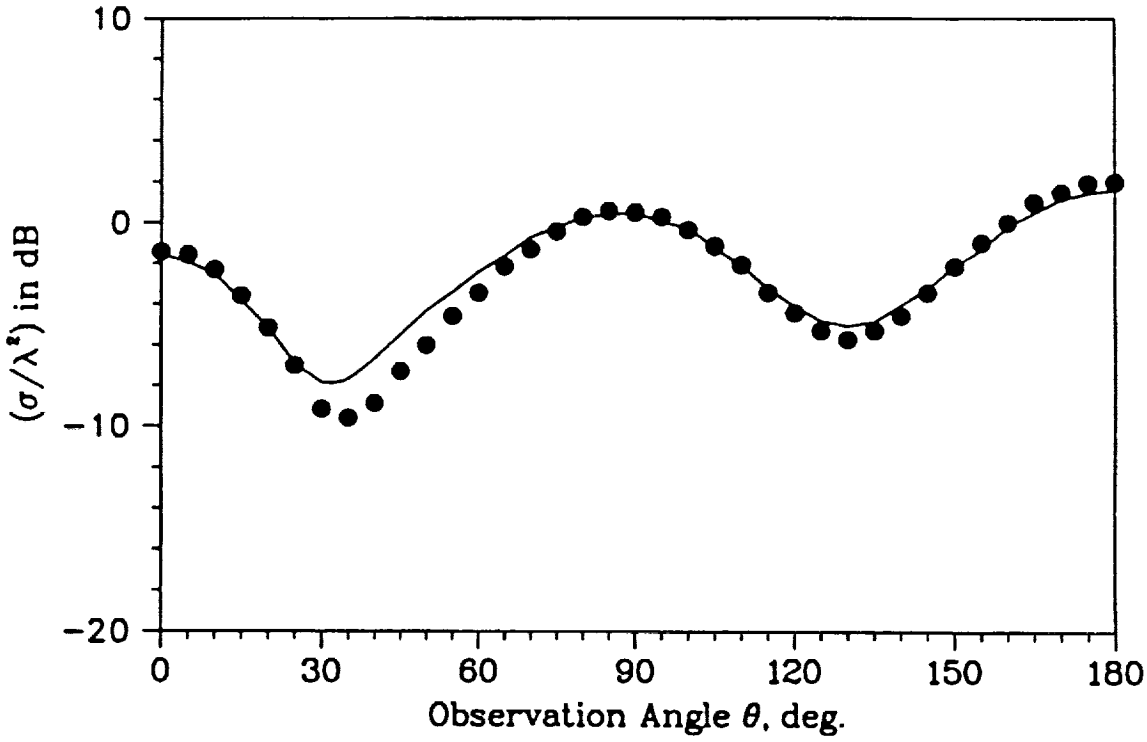

Figure 2: RCS pattern in the x-z plane for the geometry as in Figure 1, with the air-filled section replaced with dielectric having $\epsilon_r = 2 - j2$. The solid curve is the FE-ABC pattern and the black dots are MOM data for the $E_z^{\text{inc}} = 0$ polarization.

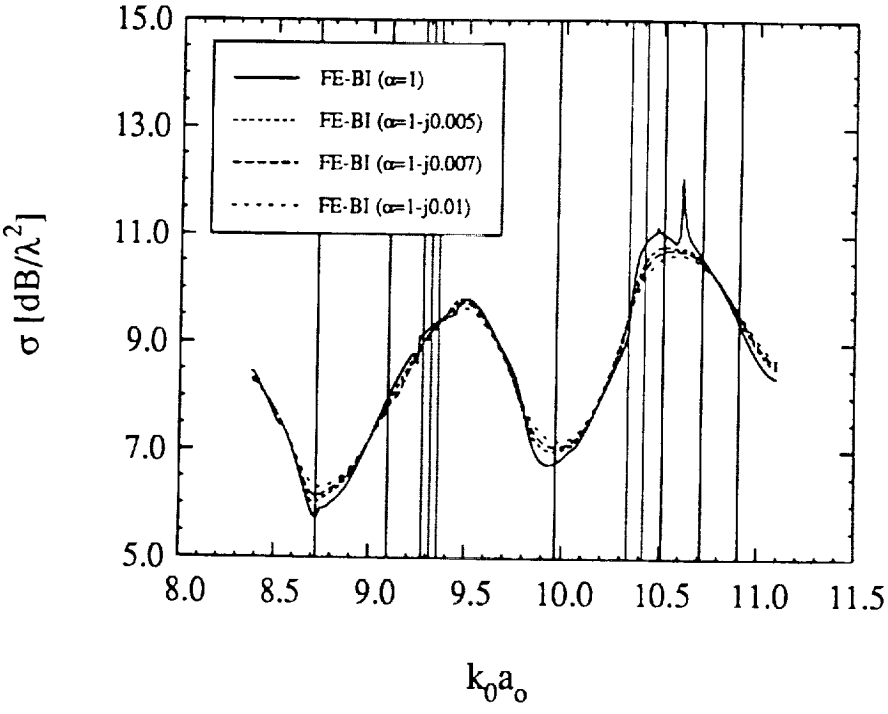

Figure 3: The axial backscatter cross section is displayed as a function of normalized radius $k_0 a_o$. The structure is a conducting sphere of radius a coated with a dielectric with $\epsilon_r = 2 - j4$ has an outer radius of $a_o = 1.02$. Employing a complex wavenumber $k = k_0\alpha$, the resonance behavior is removed for the complex values in comparison to the $\alpha = 1$ case

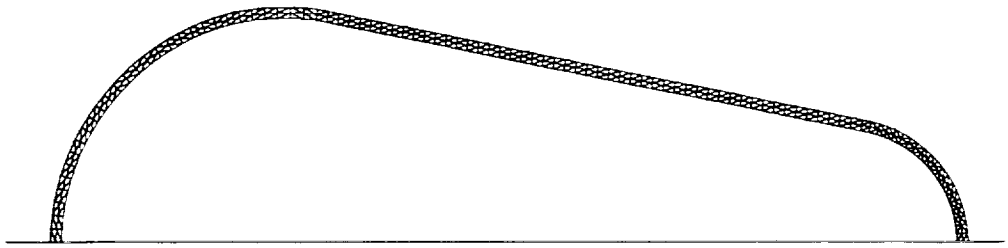

The mesh of the sphere-capped cone frustrum

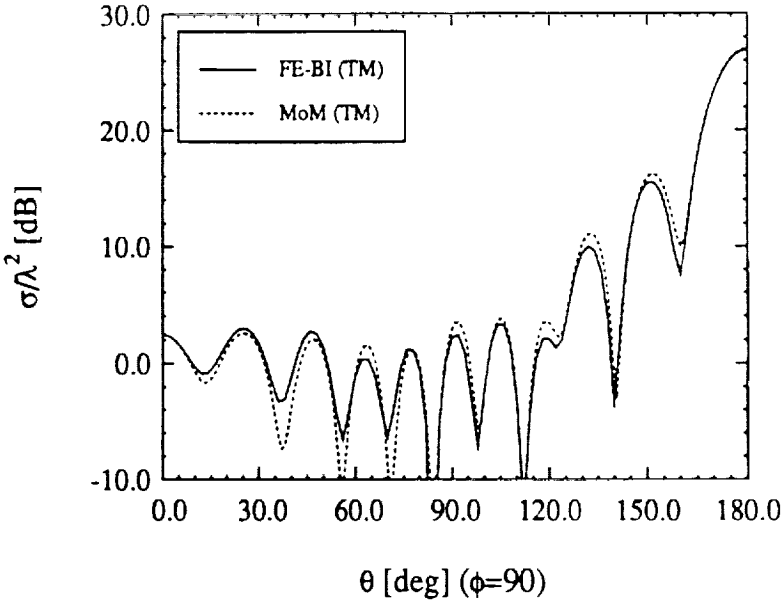

(b)

Figure 4: The bistatic scattering pattern is shown for a plane wave axially incident on the coated sphere-capped cone frustum; H-plane pattern.

(a)

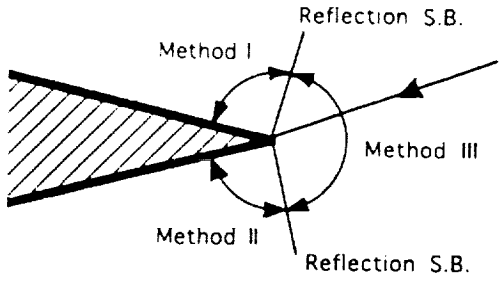

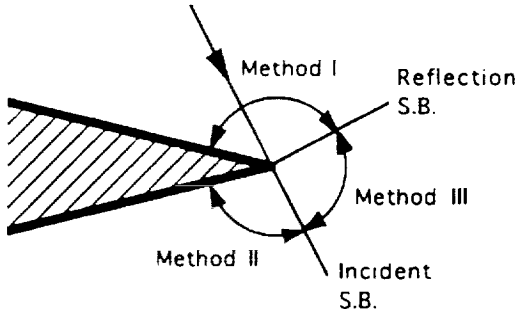

(b)

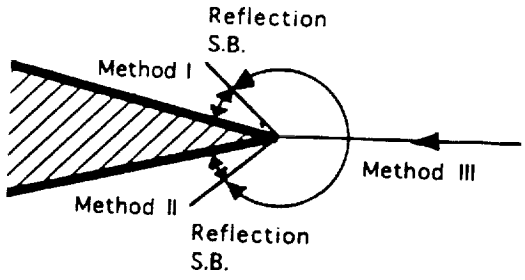

Figure 5: Different regions for the applicability of the three solutions. (a) backscatter case; (b) bistatic case.

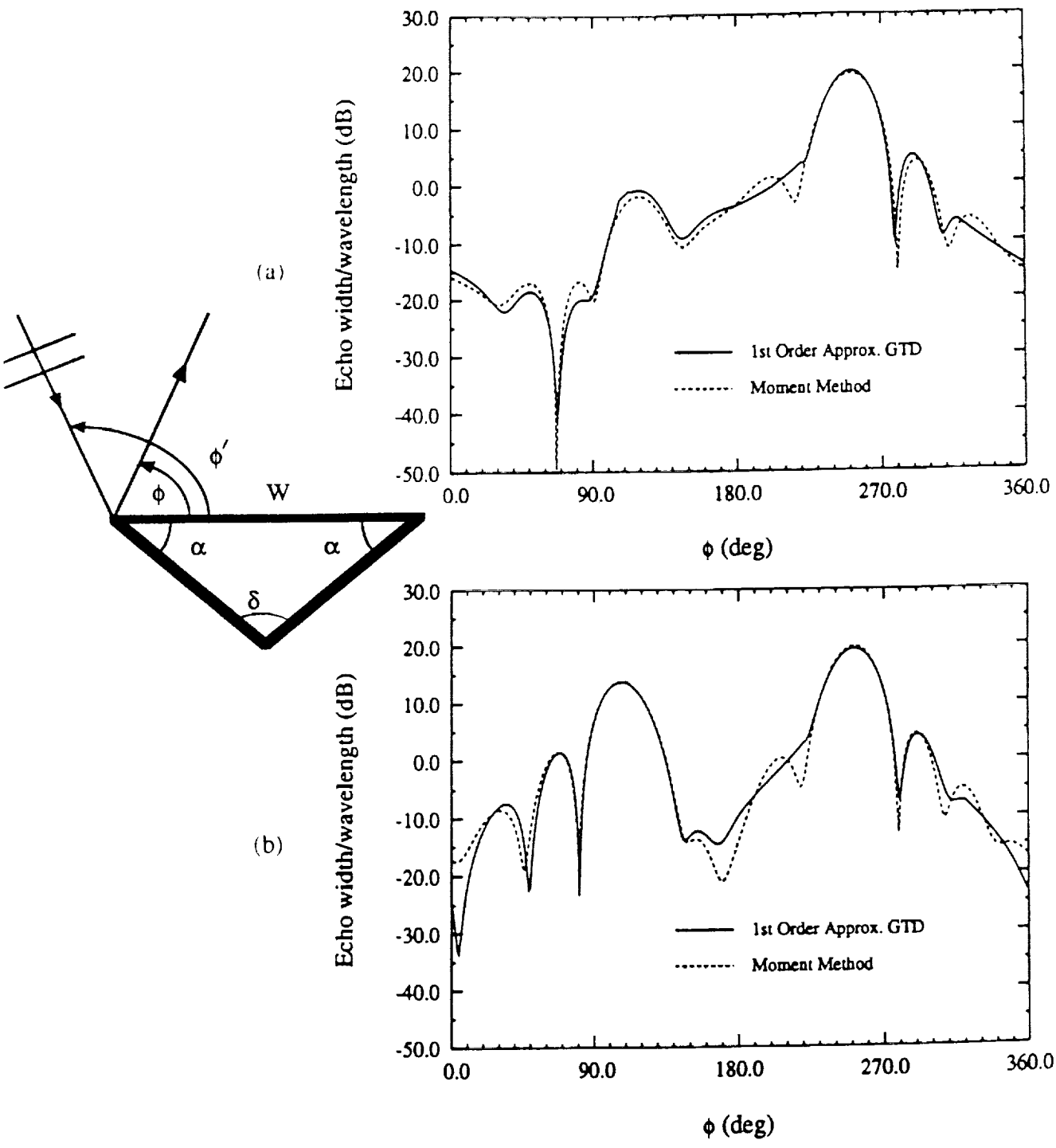

Figure 6: Far zone bistatic scattering pattern for a triangular cylinder with top side width $w = 4\lambda$, $\alpha = 40°$, $\beta_o = 30°$, $\phi' = 70°$, and its top face having $\eta = 0.5$, and the other having $\eta = 1.0 + j1.0$, (a) $E_{\beta_o\beta_o'}$, (b) $E_{\phi\phi'}$.

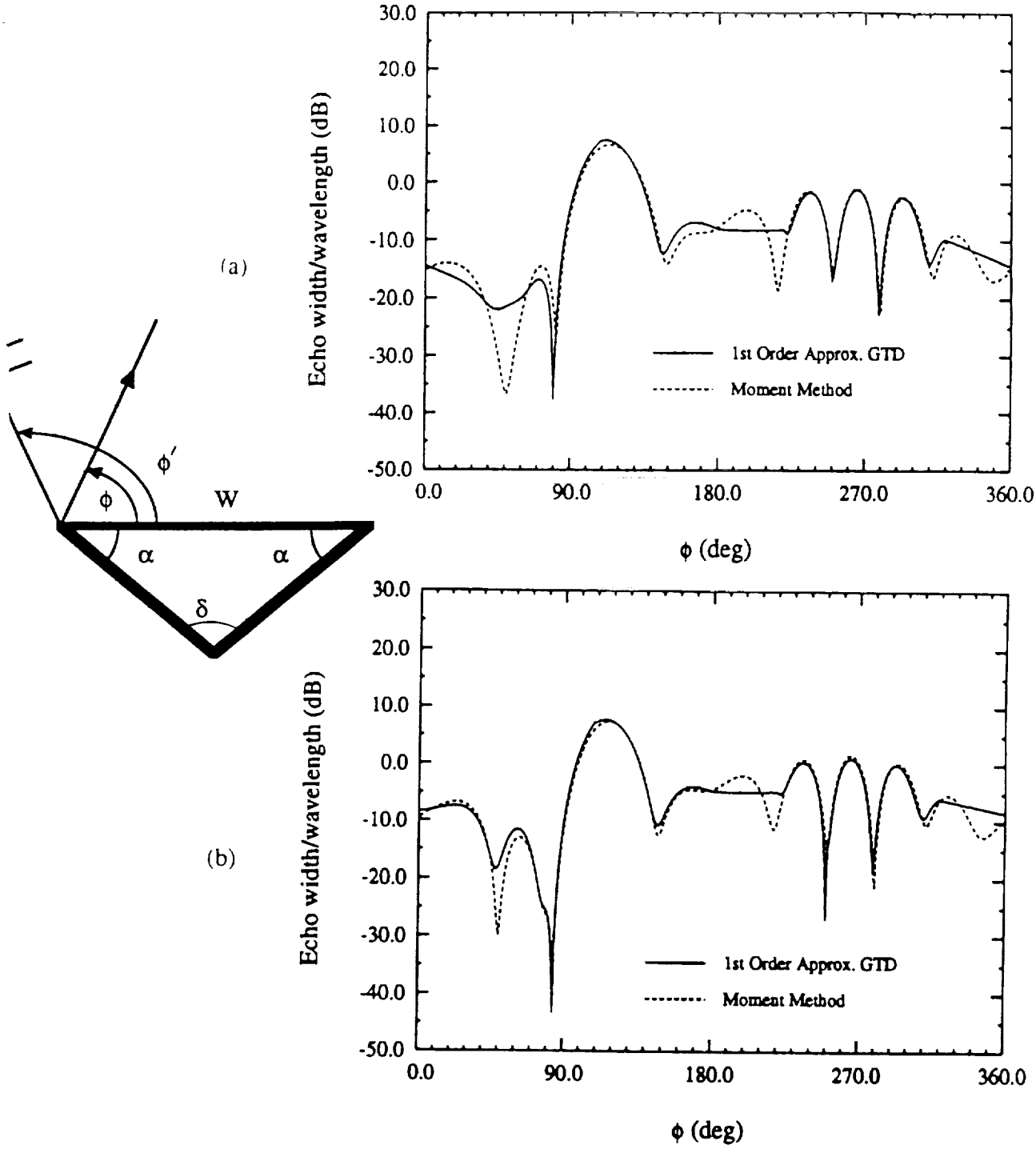

Figure 7: Far zone bistatic scattering pattern for a triangular cylinder with top side width $w = 4\lambda$, $\alpha = 40°$, $\beta_o = 30°$, $\phi' = 70°$, and its top face having $\eta = 0.5$, and the other having $\eta = 1.0 + j1.0$, (a) $E_{\phi\beta'_o}$, (b) $E_{\beta_o\phi'}$.

Appendix

FE-ATB Code attributes

- Combines the finite element method with an absorber termination boundary (FE-ATB)
- Retains geometrical fidelity
- No restriction on material composition
- Includes unique R-card and surface impedance simulation
- Yields fully sparse matrices
- Mesh terminated within $\lambda/3$ from body
- Efforts high degree of vectorization and parallelization

Comparative trends

FE-ATB Code (PEC surface)

Approx. mesh volume $V_m = 0.35 \times$ boundary surface $= 0.35S$

No. of unknowns/elements $N = 8{,}000\ V_m = 2{,}800S$ for 10 elements/λ

$20{,}000\ V_m = 7{,}000S$ for 14 elements/λ

Storage requirements:

Theoretical	27N	72,800S
Present code	44N	182,000S

Operation count 29N/iteration 8.12×10^4 S

Convergence rates have been observed to be N/50 4.6×10^6 S^2

MOM Code (PEC)

No. of unknowns: $1.5 \times 100S$ for 10 elements/λ

$1.5 \times 200S$ for 14 elements/λ

Storage requirements: $22{,}500S^2$ for 10 elements/λ

$90{,}000S^2$ for 14 elements/λ

Operation count: 3.4×10^6 S^3 for 10 elements/λ

27×10^6 S^3 for 14 elements/λ

Dielectric Cube of Side Length L

- Choose sampling rate of 10 elements/λ

FE-ATB requirements

$$\text{No. of unknowns } N \cong \left[2800\left(1+\frac{1.2}{L}\right)+1335L\right]S$$

$$\text{Storage} = 26N = 70,000\left[1+\frac{1.2}{L}+\frac{L}{2}\right]S$$

$$\text{CPU time} = 29N = 78,000\left[1+\frac{1.2}{L}+\frac{L}{2}\right]S \text{ operations/iteration}$$

MoM

$$\begin{aligned}\text{No. of unknowns } N &= (300+1335L)S\\ \text{Storage} &= (300+1335L)^2S^2\\ \text{CPU time} &= (300+1335L)^3S^3\end{aligned}$$

Examples

PEC surface $10\lambda^2$ sampled at 14 elements/λ

FE-ATB Code

No. of unknowns	= 70,000
Storage	= 1.8×10^6 words
Operation count	= 2.94×10^9

MoM code

No. of unknowns	= 3,000
Storage	= 9×10^6 words
Operation count	= 27×10^9

Dielectric Cube $L = 1.3\lambda$, $S = 10\lambda^2$ sampled at 10 elements/λ

FE-ATB code

No. of unknowns	= 71,000
Storage	= 1.85×10^6 words
Operation count	= 2.92×10^9

MoM code

No. of unknowns	= 20,350
Storage	= 0.4×10^9 words
Operation count	= 8.4×10^{12}

Number of operations vs surface area

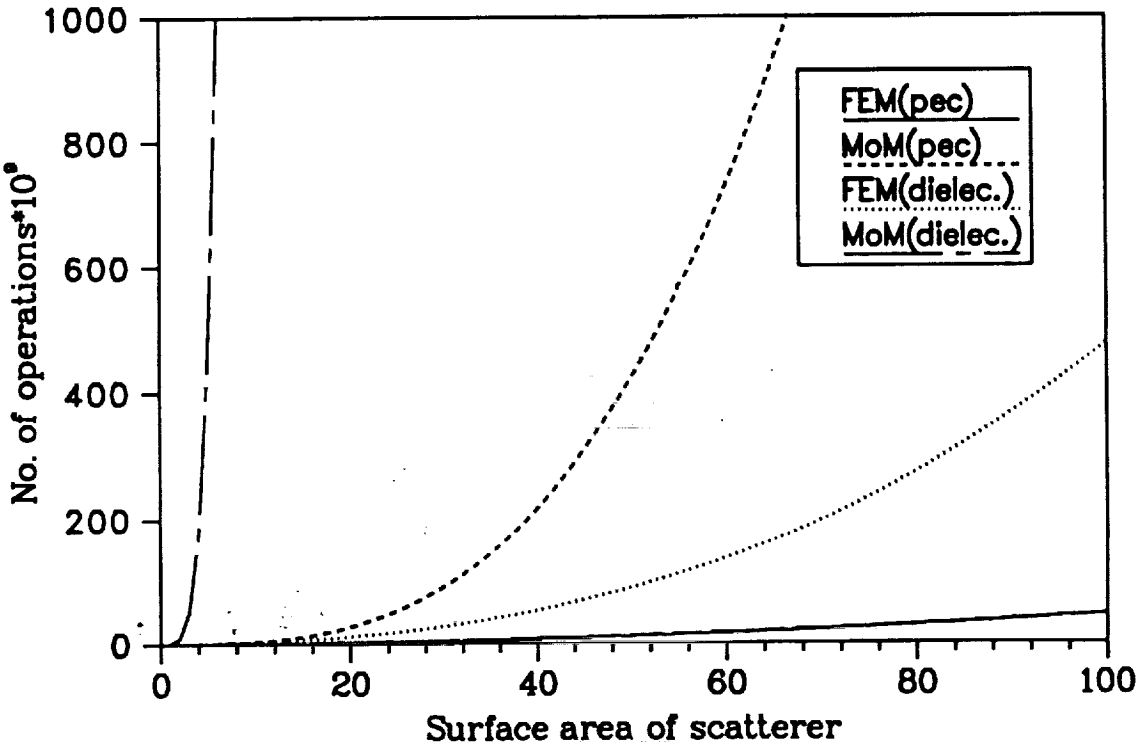

Storage requirement vs surface area

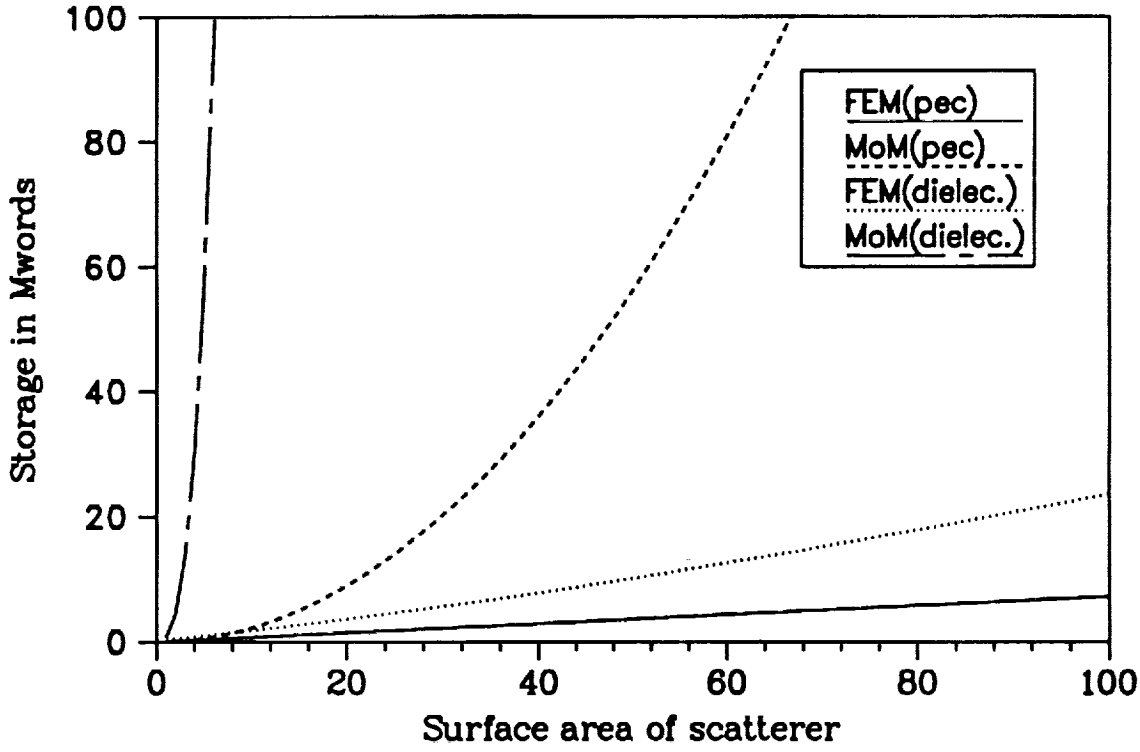

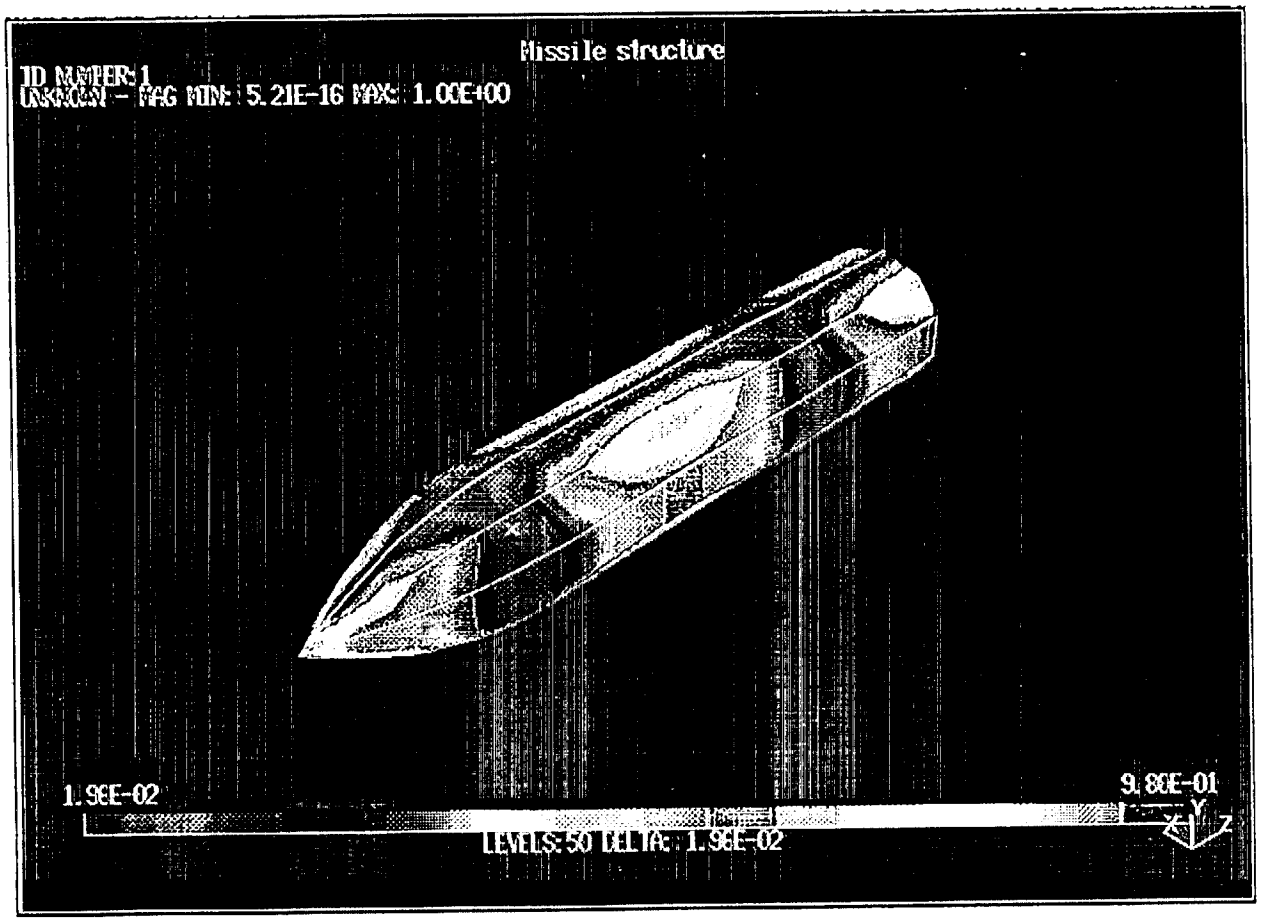
Missile structure
ID NUMBER:1
MAG MIN: 5.21E-16 MAX: 1.00E+00
1.98E-02
9.80E-01
LEVELS:50 DELTA: 1.96E-02

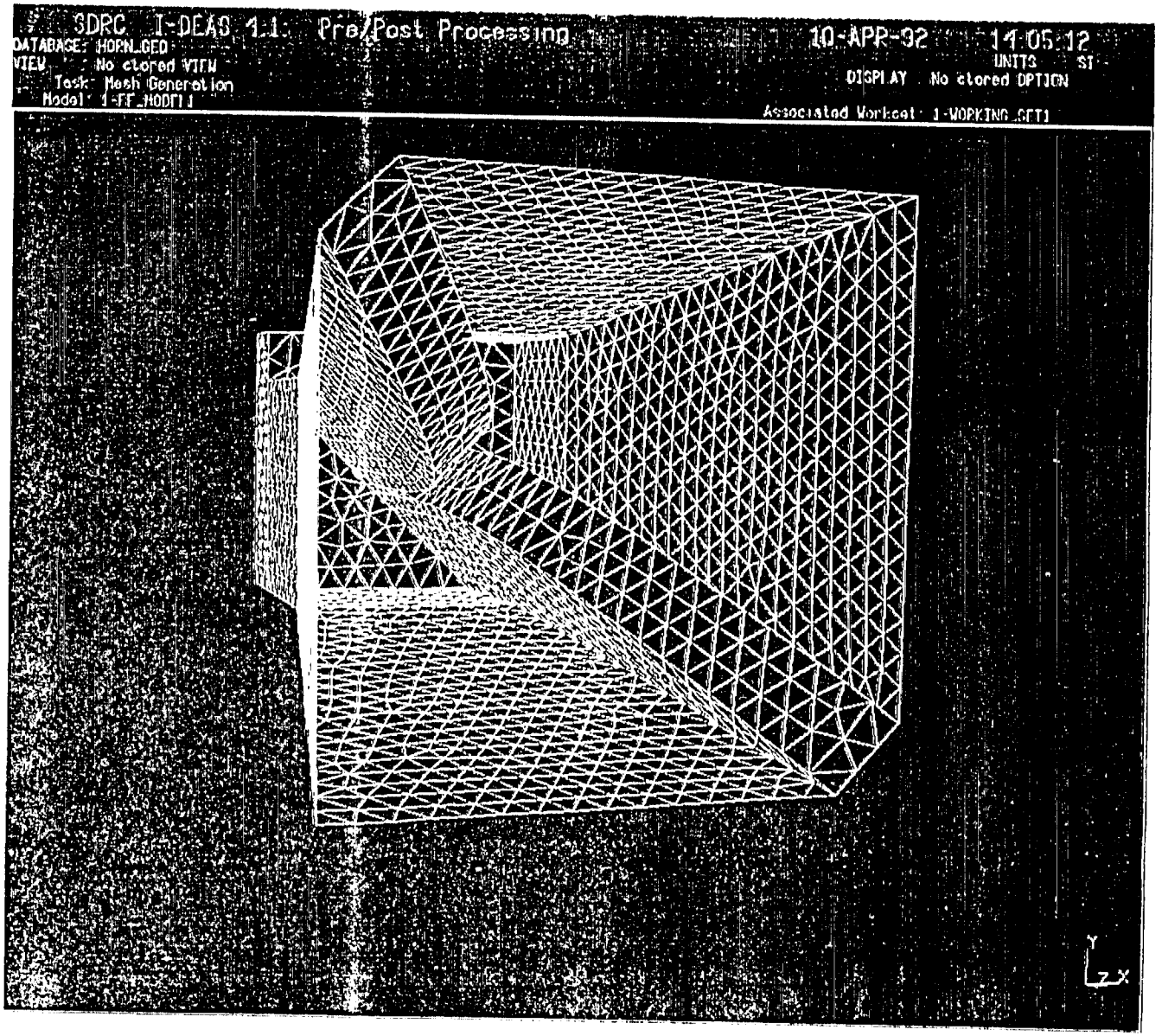
SDRC I-DEAS 1.1: Pre/Post Processing
10-APR-92 14:05:12
DATABASE: HORN_GEO
VIEW : No stored VIEW
Task: Mesh Generation
Model: 1-FF_MODEL1
UNITS SI
DISPLAY No stored OPTION
Associated Workset: 1-WORKING_SET1
Y
Z
X

Memorandum

Discretization of the new integral equation for modelling inhomogeneous dielectrics

Sunil S.Bindiganavale and John L.Volakis

Radiation Laboratory
Department of Electrical Engineering
and Computer Science
The University of Michigan
Ann Arbor, Michigan 48109-2122.

September 5,1992

Abstract

A new integral equation for scattering by an inhomogeneous dielectric is discretized using rectangular brick elements. Edge-based linear shape functions are used for the expansion of the field inside the dielectric and the modified Galerkin's technique is employed for testing the integral equation. Results demonstrating the validity of the integral equation are presented.

1 Introduction

The modeling of inhomogeneous dielectrics by an integral equation approach is traditionally accomplished by the introduction of equivalent volume electric and magnetic currents as shown in figure (1).

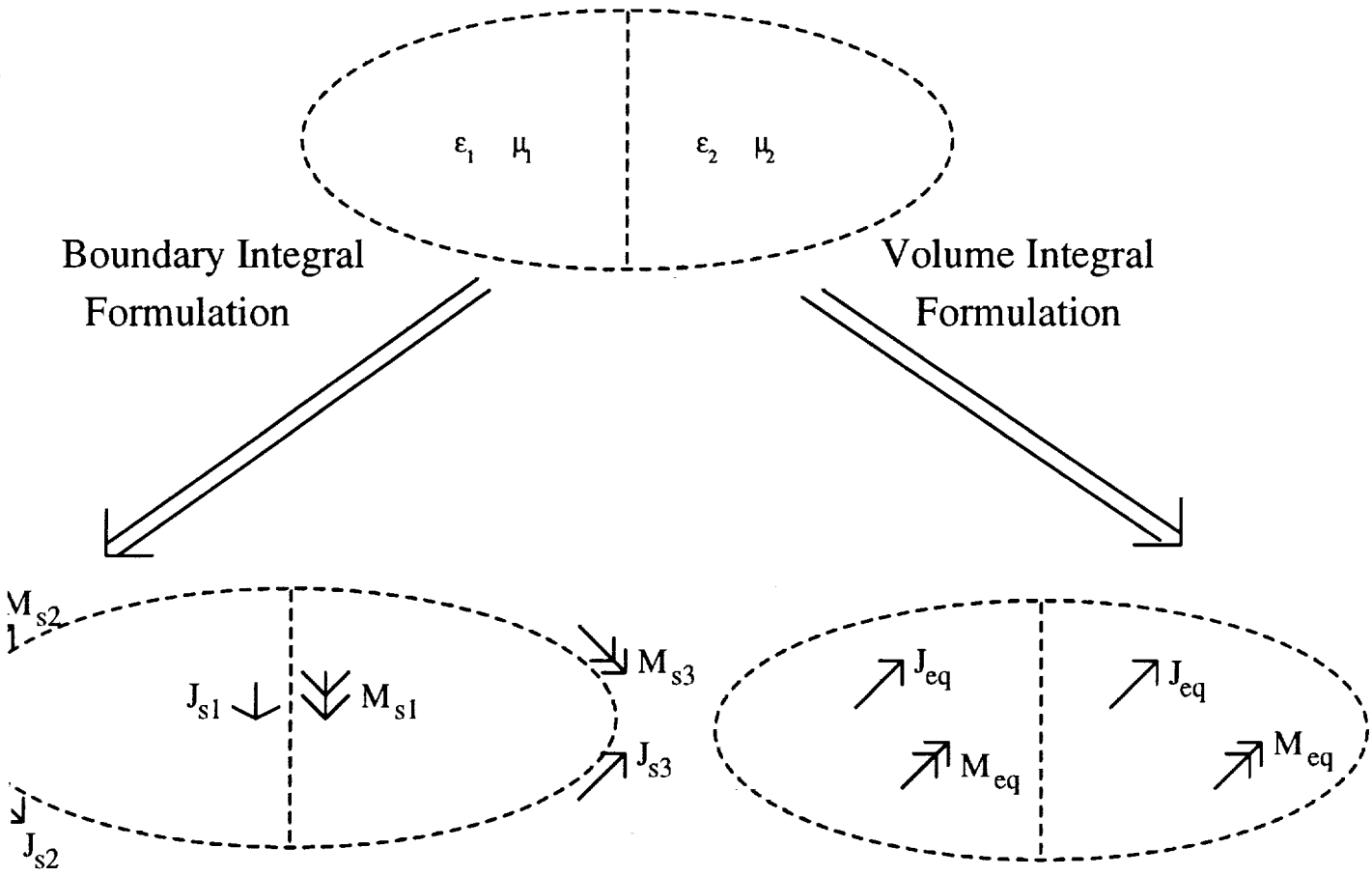

Figure 1: Traditional Dielectric/Ferrite body formulation

For a dielectric with non-trivial permittivity and permeability this type of modeling implies six scalar unknowns at each volume location. As a result, the implementation of the resulting integral equation is computationally intensive and has excessive storage requirements. Recently [1] it was demonstrated that any inhomogeneous dielectric material, regardless of its permittivity and permeability profile can be modelled by a single electric or magnetic current density. Alternatively, either the electric or magnetic fields within the dielectric can be used as the unknown quantities. However,

since this reduced-unknown integral equation involves the derivatives of the unknown quantities, a higher basis function is required for discretizing the resulting integral equation. Hence the use of linear shape functions.

2 Discretization

2.1 The Integral equation

The volume electric-field integral equation to be discretized is of the form :

$$\begin{aligned}\mathbf{E}^i(\mathbf{r}) &= \mathbf{E}(\mathbf{r}) - \iiint_{V_d} \left[\nabla G_0(\mathbf{r},\mathbf{r}') \times \bar{\mathbf{I}}\right] \cdot \left\{ \frac{\mu_r - 1}{\mu_r} \nabla' \times \mathbf{E}(\mathbf{r}') \right. \\ &\quad \left. + \nabla' \times [(\epsilon_r - 1)\mathbf{E}(\mathbf{r}')] \right\} dv' \end{aligned} \tag{1}$$

where $\bar{\mathbf{I}} = \hat{x}\hat{x} + \hat{y}\hat{y} + \hat{z}\hat{z}$, $G_0(\mathbf{r},\mathbf{r}')$ is the free-space Green's function, $\mathbf{E}^i$ is the incident field and V_d is the dielectric volume.
From the properties of an identity dyad, equation (1) becomes

$$\begin{aligned}\mathbf{E}^i(\mathbf{r}) &= \mathbf{E}(\mathbf{r}) + \iiint_{V_d} \nabla G_0(\mathbf{r},\mathbf{r}') \times \left\{ \frac{\mu_r - 1}{\mu_r} \nabla' \times \mathbf{E}(\mathbf{r}') \right. \\ &\quad \left. + \nabla' \times [(\epsilon_r - 1)\mathbf{E}(\mathbf{r}')] \right\} dv' \end{aligned} \tag{2}$$

Assuming the material parameters are constant in each unit cell of discretization and the domain of integration is limited to one such cell (say cell 'q') then equation (2) is :

$$\mathbf{E}^i(\mathbf{r}) = \mathbf{E}(\mathbf{r}) + \left\{ \epsilon_{rq} - \frac{1}{\mu_{rq}} \right\} \iiint_{V_q} \nabla G_0(\mathbf{r},\mathbf{r}') \times [\nabla' \times \mathbf{E}(\mathbf{r}')]\, dv' \tag{3}$$

where μ_{rq} and ϵ_{rq} are the relative permeability and permittivity within the qth cell and V_q is the volume of the qth cell.
From elementary calculus,

$$\nabla G_0(\mathbf{r},\mathbf{r}') = -\left(jk_0 + \frac{1}{R}\right) G_0(\mathbf{r},\mathbf{r}')\hat{R} \tag{4}$$

Hence equation (3) becomes:

$$\mathbf{E}^i(\mathbf{r}) = \mathbf{E}(\mathbf{r}) - \left\{\epsilon_{rq} - \frac{1}{\mu_{rq}}\right\} \iiint_{V_q} \left(jk_0 + \frac{1}{R}\right) G_0(\mathbf{r},\mathbf{r}') \hat{R} \times [\nabla' \times \mathbf{E}(\mathbf{r}')]\, dv' \quad (5)$$

2.2 Basis functions

The dielectric layer is assumed to be thin (t $\ll \lambda$). It is discretized by use of rectangular brick elements whose height is equal to the thickness of the dielectric. For the expansion of the field inside the dielectric we use edge-based expansion functions borrowed from the finite element domain [2]. Edge-based expansion functions avoid explicit specification of the fields at the corners and edges. The geometry of the brick element with a local co-ordinate system is shown in figure (2). The electric field can be expanded

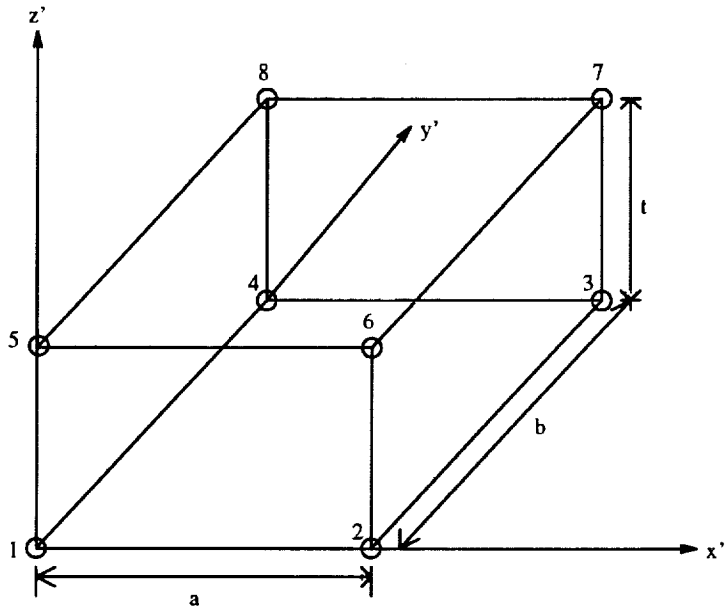

Figure 2: The rectangular brick element

as :

$$\mathbf{E}(\mathbf{r}') = \sum_{e=1}^{N}\left\{\hat{x}\sum_{j=1}^{4} W_{xj}^{e}(y',z')\phi_{xj}^{e} + \hat{y}\sum_{j=1}^{4} W_{yj}^{e}(z',x')\phi_{yj}^{e} + \hat{z}\sum_{j=1}^{4} W_{zj}^{e}(x',y')\phi_{zj}^{e}\right\} \tag{6}$$

where

$$W_{x1}^{e} = \frac{(b-y')(t-z')}{bt} \qquad W_{x2}^{e} = \frac{(y')(t-z')}{bt}$$

$$W_{x3}^{e} = \frac{(b-y')(z')}{bt} \qquad W_{x4}^{e} = \frac{(y')(z')}{bt}$$

$$W_{y1}^{e} = \frac{(t-z')(a-x')}{ta} \qquad W_{y2}^{e} = \frac{(z')(a-x')}{ta}$$

$$W_{y3}^{e} = \frac{(t-z')(x')}{ta} \qquad W_{y4}^{e} = \frac{(z')(x')}{ta}$$

$$W_{z1}^{e} = \frac{(a-x')(b-y')}{ab} \qquad W_{z2}^{e} = \frac{(x')(b-y')}{ab}$$

$$W_{z3}^{e} = \frac{(a-x')(y')}{ab} \qquad W_{z4}^{e} = \frac{(x')(y')}{ab}$$

Expanding equation (5) in terms of one such vector expansion function :

$$\mathbf{E}^{i}(\mathbf{r}) = \mathbf{W}_{n}^{q}(\mathbf{r}) - \left\{\epsilon_{rq} - \frac{1}{\mu_{rq}}\right\}\iiint_{V_q}\left(jk_0 + \frac{1}{R}\right)G_0(\mathbf{r},\mathbf{r}')\,\hat{R}\times\left[\nabla'\times\mathbf{W}_{q}^{n}(\mathbf{r}')\right]dv' \tag{7}$$

2.3 Testing procedure

Galerkin's procedure involves choosing the weighting (testing) functions to be the same as basis functions in the inner product of the method-of-moments solution as follows :

$$\langle \mathbf{w}, \mathbf{g} \rangle = \iiint_V \mathbf{w} \cdot \mathbf{g}\, dv = \iiint_{V_p} \mathbf{f} \cdot \mathbf{g}\, dv \tag{8}$$

where w and f are the weighting and basis functions respectively, and this integration is over the whole volume of the dielectric. Since the basis functions are subdomain basis functions, the integration limits of equation (8) actually can be reduced to V_p, the volume of the cell p where the weighting function w is defined. Forming the above scalar product on equation (7):

$$\begin{aligned} \iiint_{V_p} \mathbf{W}_m^p(\mathbf{r}) \cdot \mathbf{E}^i(\mathbf{r})\, dv \;=\; & \left[\iiint_{V_p} \mathbf{W}_m^p(\mathbf{r}) \cdot \mathbf{W}_n^q(\mathbf{r}')\, dv\right] \delta(p-q) - \left\{\epsilon_{rq} - \frac{1}{\mu_{rq}}\right\} \\ & \iiint_{V_p} \mathbf{W}_m^p(\mathbf{r}) \cdot \iiint_{V_q} \left(jk_0 + \frac{1}{R}\right) G_0(\mathbf{r}, \mathbf{r}') \\ & \hat{R} \times \left[\nabla' \times \mathbf{W}_q^n(\mathbf{r}')\right] dv'\, dv \end{aligned} \tag{9}$$

where $\delta(p-q)$ indicates a contribution within the self-cell alone. Equation (9) gives rise to a system of equations which can be written as:

$$\{Z_{mn}\}\{\phi_n\} = \{V_m\}$$

where typical elements are given by :

$$V_m^p = \iiint_{V_p} \mathbf{W}_m^p(\mathbf{r}) \cdot \mathbf{E}^i(\mathbf{r})\, dv$$

$$\begin{aligned} Z_{mn}^{pq} \;=\; & \left[\iiint_{V_p} \mathbf{W}_m^p(\mathbf{r}) \cdot \mathbf{W}_n^q(\mathbf{r}')\, dv\right] \delta(p-q) - \left\{\epsilon_{rq} - \frac{1}{\mu_{rq}}\right\} \\ & \iiint_{V_p} \mathbf{W}_m^p(\mathbf{r}) \cdot \iiint_{V_q} \left(jk_0 + \frac{1}{R}\right) G_0(\mathbf{r}, \mathbf{r}') \\ & \hat{R} \times \left[\nabla' \times \mathbf{W}_q^n(\mathbf{r}')\right] dv' \end{aligned} \tag{10}$$

For self-cells the kernel of the integrand in equation (3) has a $\frac{1}{R^2}$ singularity which needs to be carefully evaluated. For self-cells we re-write the corresponding impedance matrix element from equation (3) as :

$$Z_{mn}^{pq} = \left[\iiint_{V_p} \mathbf{W}_m^p(\mathbf{r}) \cdot \mathbf{W}_n^q(\mathbf{r}')\, dv\right] \delta(p-q) + \left\{\epsilon_{rq} - \frac{1}{\mu_{rq}}\right\} \iiint_{V_q} (\nabla' \times \mathbf{W}_q^n(\mathbf{r}')) \cdot \iiint_{V_p} \mathbf{W}_m^p(\mathbf{r}) \times \nabla G_0(\mathbf{r}, \mathbf{r}')\, dv\, dv' \quad (11)$$

The symmetric property of the free-space Green's function gives

$$\nabla G_0(\mathbf{r}, \mathbf{r}') = -\nabla' G_0(\mathbf{r}, \mathbf{r}') \quad (12)$$

Using equation (12) and interchanging the order of integration in equation (11) :

$$\begin{aligned} Z_{mn}^{pq} = {} & \left[\iiint_{V_p} \mathbf{W}_m^p(\mathbf{r}) \cdot \mathbf{W}_n^q(\mathbf{r}')\, dv\right] \delta(p-q) + \left\{\epsilon_{rq} - \frac{1}{\mu_{rq}}\right\} \\ & \iiint_{V_q} \left(\nabla' \times \mathbf{W}_q^n(\mathbf{r}')\right) \cdot \iiint_{V_p} [\mathbf{W}_m^p(\mathbf{r}) - \mathbf{W}_m^p(\mathbf{r}')] \times \nabla G_0(\mathbf{r}, \mathbf{r}')\, dv\, dv' \\ & - \left\{\epsilon_{rq} - \frac{1}{\mu_{rq}}\right\} \\ & \iiint_{V_q} \left(\nabla' \times \mathbf{W}_q^n(\mathbf{r}')\right) \cdot \left\{\mathbf{W}_m^p(\mathbf{r}') \times \nabla' \iiint_{V_p} G_0(\mathbf{r}, \mathbf{r}')\, dv\right\} dv' \end{aligned} \quad (13)$$

An analytical expression for the integration of the free-space Green's function over an equivalent spherical volume is derived based on [3]. This is of the form :

$$\begin{aligned} \iiint_{V_p} G_0(\mathbf{r}, \mathbf{r}')\, dv = {} & \frac{1}{k_0^2 s_0}\left\{e^{-jk_0 s_0}\left(\frac{\sin(k_0 s_0)}{k_0} - s_0 \cos(k_0 s_0)\right) + \sin(k_0 s_0) e^{-jk_0 \eta}\right. \\ & \left.\left(\frac{1}{k_0} + j\eta\right) - \sin(k_0 s_0) e^{-jk_0 s_0}\left(\frac{1}{k_0} + j s_0\right)\right\} \end{aligned} \quad (14)$$

where η is the radius of a sphere equal in volume to the rectangular brick and s_0 is the distance between the center of the sphere and the source point, $\mathbf{r}'$. The name modified Galerkin's method (MGM) comes from the fact that the testing cells are spheres while the source cells continue to be the original

rectangular bricks. Note that the MGM is not equivalent to using spherical cells because we continue to use rectangular bricks as the domain for the source integration.
Also,

$$\nabla' \iiint_{V_p} G_0(\mathbf{r},\mathbf{r}')\,dv = \left\{ \frac{[k_0 s_0 \cos(k_0 s_0) - \sin(k_0 s_0)]}{k_0^3 s_0^2 e^{jk_0\eta}} + \frac{j\eta\,[k_0 s_0 \cos(k_0 s_0) - \sin(k_0 s_0)]}{k_0^2 s_0^2 e^{jk_0\eta}} \right\} \left\{ \frac{\hat{x}(x-x_c) + \hat{y}(y-y_c) + \hat{z}(z-z_c)}{s_0} \right\} \quad (15)$$

where (x_c, y_c, z_c) are the co-ordinates of the center of the sphere. Note that as $s_0 \to 0$ all the terms in equations (14) and (15) converge to a finite quantity.

2.4 Excitation

In all the above cases, the excitation is a plane wave given by

$$\mathbf{E}^i(\mathbf{r}) = \left[\left(\hat{\alpha}\cdot\hat{\theta}^i\right)\hat{\theta}^i + \left(\hat{\alpha}\cdot\hat{\phi}^i\right)\hat{\phi}^i \right] e^{-j\mathbf{k}^i\cdot\mathbf{r}} \quad (16)$$

where $\hat{\alpha} = \hat{\theta}^i \cos\alpha + \hat{\phi}^i \sin\alpha$ is the polarization vector given by

$$\mathbf{k}^i = -k_0 \left(\sin\theta^i \cos\phi^i \hat{x} + \sin\theta^i \sin\phi^i \hat{y} + \cos\theta^i \hat{z} \right) \quad (17)$$

and $\hat{\theta}^i$ and $\hat{\phi}^i$ are the usual unit vectors in the spherical system and are associated with the angles θ^i and ϕ^i.

2.5 Scattering parameters

The scattered field can be obtained from equation (2) and (4) as

$$\mathbf{E}^s(\mathbf{r}) = \iiint_{V_d} \nabla G_0(\mathbf{r},\mathbf{r}') \times \left\{ \frac{\mu_r - 1}{\mu_r} \nabla' \times \mathbf{E}(\mathbf{r}') + \nabla' \times [(\epsilon_r - 1)\mathbf{E}(\mathbf{r}')] \right\} dv' \quad (18)$$

Making the far field approximation for the magnitude $R \approx r$ and the phase $R \approx r - \hat{r}\cdot\mathbf{r}'$,

$$\mathbf{E}^s(\mathbf{r}) = \frac{jk_0 e^{-jk_0 r}}{4\pi r} \sum_{q=1}^{N} \left\{ \epsilon_{rq} - \frac{1}{\mu_{rq}} \right\} \iiint_{V_q} e^{jk_0 \hat{r}\cdot\mathbf{r}'} \left[\hat{r} \times \nabla' \times \mathbf{E}(\mathbf{r}')\right] dv' \quad (19)$$

Then the RCS is given by :

$$\sigma = \lim_{r\to\infty} 4\pi r^2 \frac{|\mathbf{E}^s(\mathbf{r})|^2}{|\mathbf{E}^i(\mathbf{r})|^2} \tag{20}$$

3 Results and Validation

The implementation of the presented numerical solution is lengthy as is usually the case with most three-dimensional numerical solutions. The validation of the code was done with data obtained from codes used to generate the results in [4]. Figure (3) displays the backscatter patterns for a 0.2λ long, 0.2λ wide and 0.025λ thick dielectric plate. Figures (4) and (5) display backscatter patterns for 0.1λ long, 0.1λ wide and 0.025λ thick and 0.2λ long, 0.2λ wide and 0.025λ thick dielectric/magnetic plates respectively. Figure (6) shows bistatic scattering patterns for a 0.2λ long, 0.2λ wide and 0.025λ thick PEC block simulated by a lossy dielectric.

4 Conclusion

In this work we discretized and implemented a new, reduced unknown integral equation for scattering by a dielectric layer. Results demonstrating the validity of the integral equation were presented. The impedance matrix generated was found to be asymmetric since the testing procedure destroys the reciprocity of the integral equation. Hence iterative schemes like the CGFFT for rectangular plates could not be employed; thereby limiting the size of the structures investigated. Modified forms of this integral equation which result in symmetric impedance matrices are being investigated.

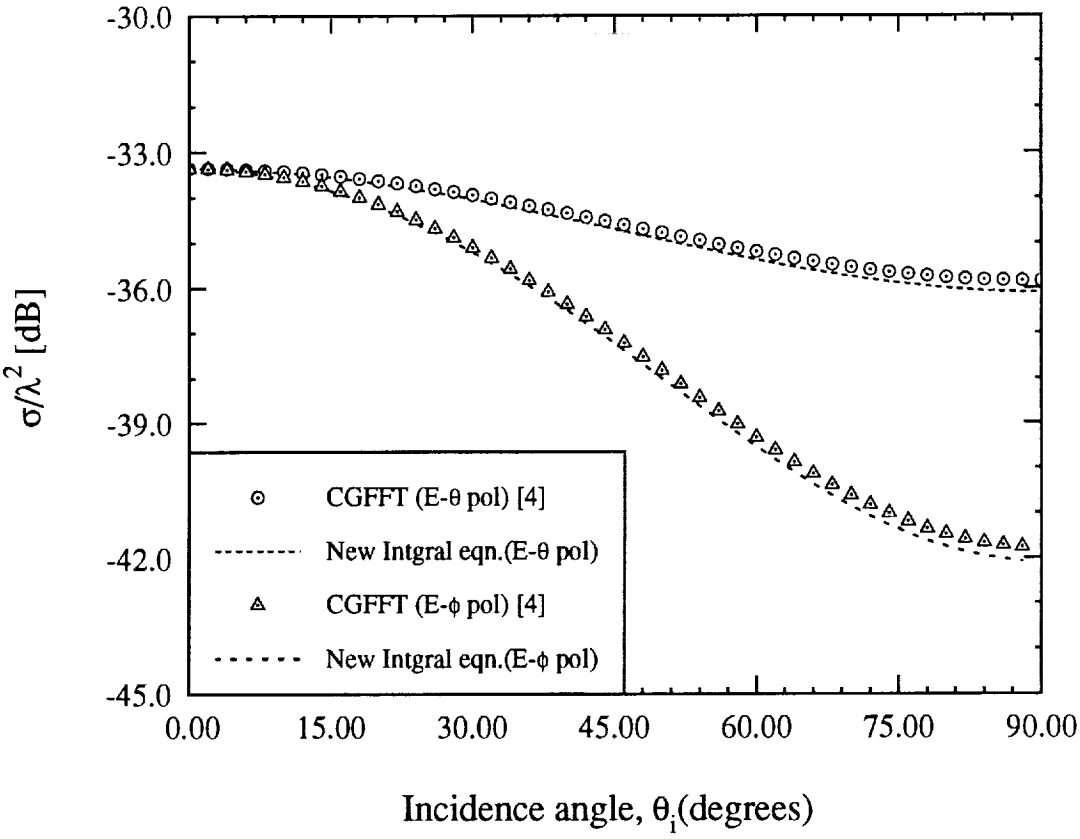

Figure 3: Backscatter RCS for l=0.2λ, w=0.2λ and t=0.025λ dielectric plate ($\epsilon_r = 2 - j2, \mu_r = 1$)

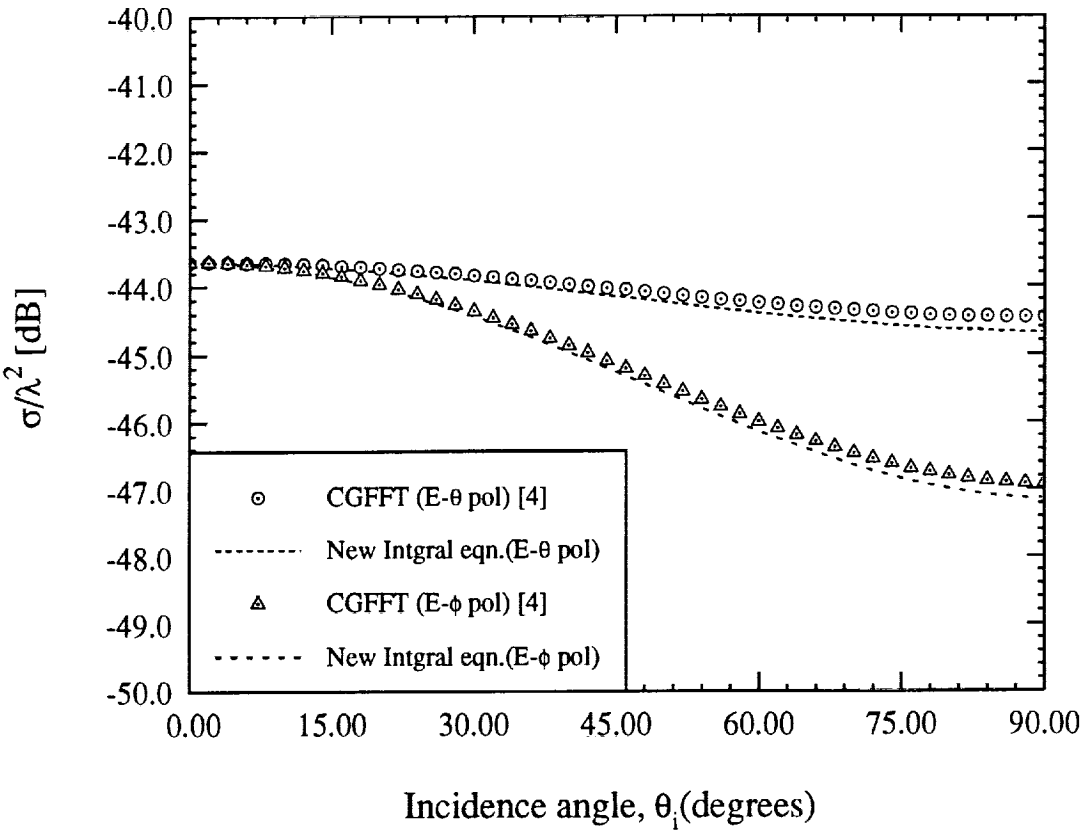

Figure 4: Backscatter RCS for l=0.1λ, w=0.1λ and t=0.025λ dielectric/magnetic plate ($\epsilon_r = 7.4 - j1.11, \mu_r = 1.4 - j0.672$)

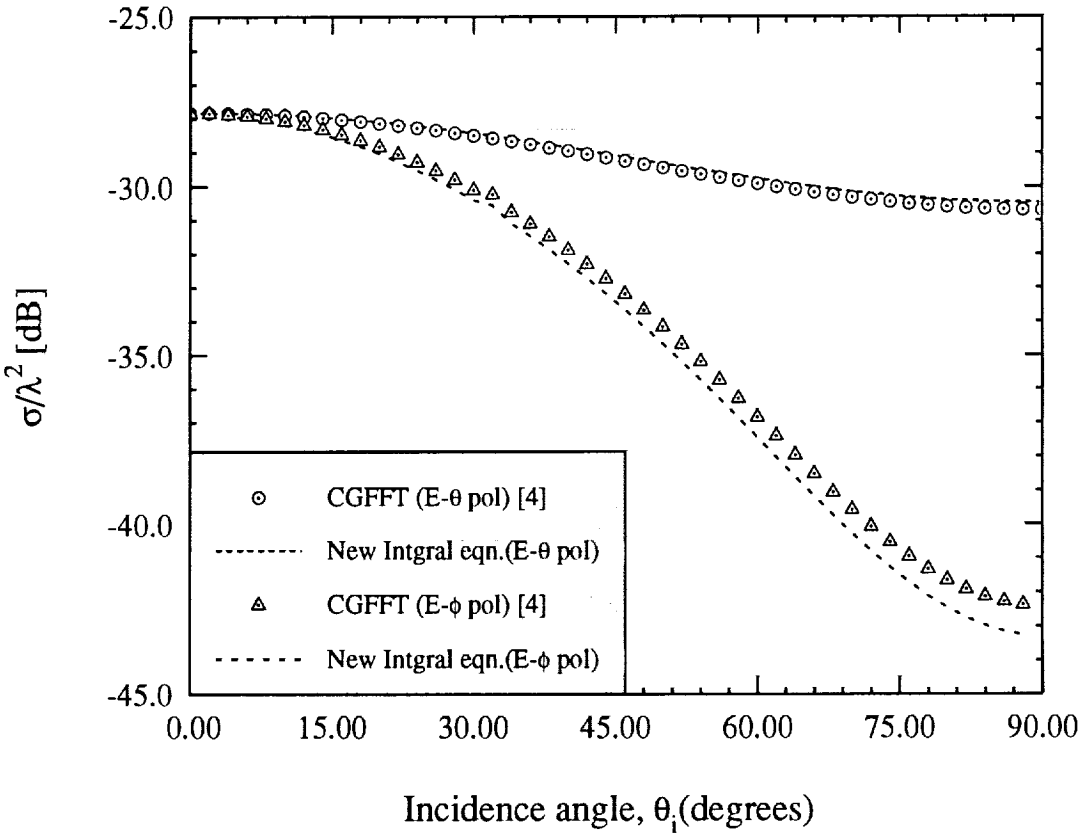

Figure 5: Backscatter RCS for l=0.2λ, w=0.2λ and t=0.025λ dielectric/magnetic plate ($\epsilon_r = 7.4 - j1.11, \mu_r = 1.4 - j0.672$)

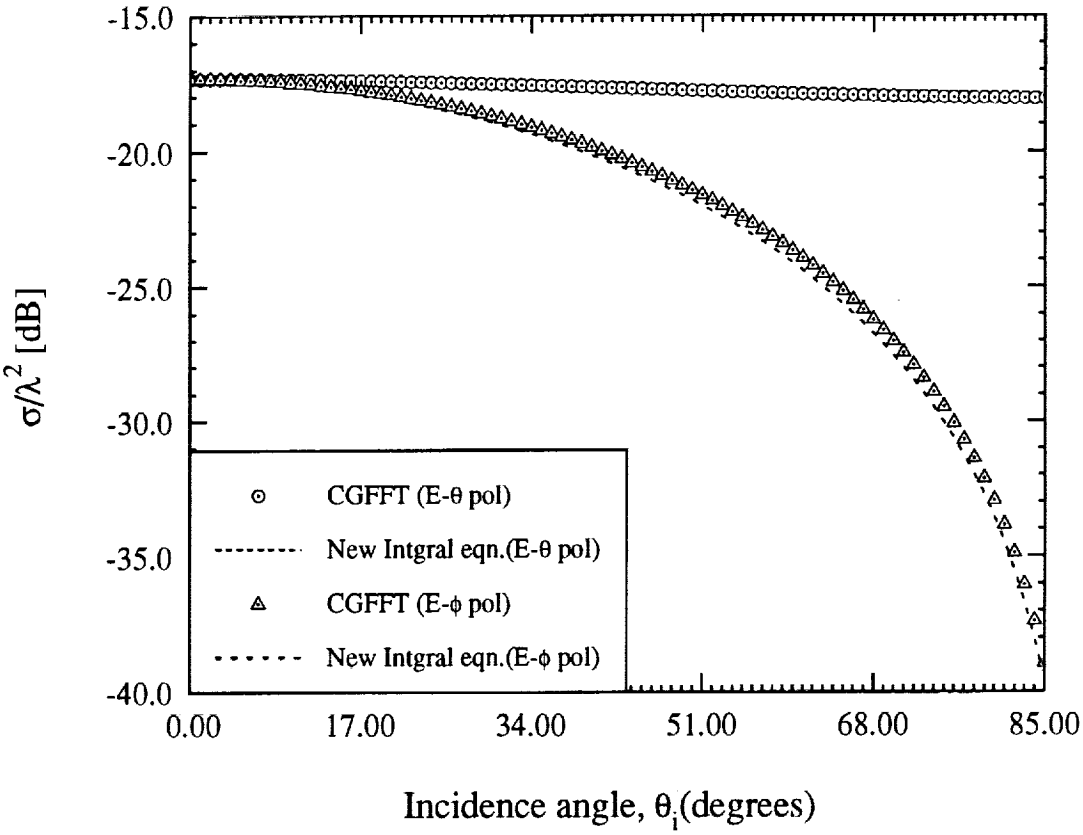

Figure 6: Bistatic RCS for l=0.2λ, w=0.2λ and t=0.025λ PEC simulated by lossy dielectric ($\epsilon_r = 1 - j100, \mu_r = 1$)

References

[1] J.L.Volakis, "Alternative field representations and integral equations for modeling inhomogeneous dielectrics," *IEEE Trans. Microwave Theory Techn.*, vol.40, no.3, pp.604-608, March 1992.

[2] J.M.Jin and J.L.Volakis, "Electromagnetic scattering by and transmission through a three-dimensional slot

in a thick conducting plane," *IEEE Trans. Antennas Propagat.*, vol.39, no.1, pp.543-550, Apr.1991.

[3] C.T.Tsai, H.Massoudi, C.H.Durney and M.F.Iskander, "A procedure for calculating fields inside arbitarily shaped inhomogeneous dielectric bodies using linear basis functions with the moment method," *IEEE Trans. Microwave Theory Techn.*, vol.34, no.11, pp.1131-1139, November 1986.

[4] T.J.Peters and J.L.Volakis, "Application of a conjugate gradient FFT method to scattering from thin planar material plates," *IEEE Trans. Antennas Propagat.*, vol.36, no.4, pp.518-526, Apr.1988.